Nonequilibrium dynamics of an ultracold dipolar gas

A. G. Sykes and J. L. Bohn
JILA, University of Colorado and National Institute of Standards and Technology, Boulder, Colorado 80309-0440, USA
(Received 7 November 2014; published 23 January 2015)

We study the relaxation and damping dynamics of an ultracold, but not quantum degenerate, gas consisting of dipolar particles. These simulations are performed using a direct simulation Monte Carlo method and employing the highly anisotropic differential cross section of dipoles in the Wigner threshold regime. We find that both cross-dimensional relaxation and damping of breathing modes occur at rates that are strongly dependent on the orientation of the dipole moments relative to the trap axis. The relaxation simulations are in excellent agreement with recent experimental results in erbium. The results direct our interest toward a less explored regime in dipolar gases where interactions are dominated by collision processes rather than mean-field interactions.

DOI: 10.1103/PhysRevA.91.013625 PACS number(s): 67.85.−d, 47.45.Ab, 05.20.Dd

I. INTRODUCTION

Much of the research on ultracold dipolar gases has heretofore focused on the quantum degenerate regime, where dipolar interactions can significantly influence the behavior of the gas through the mean field. Aspects of this influence include changing the shape and mechanical stability of the gas [1–5], as well as altering the excitation spectrum to include low-energy roton modes in a Bose-Einstein condensate [6–9]. A host of related phenomena have been predicted and observed [10–13], driven by the direct action of the long-ranged, anisotropic dipolar interaction on the particles' motion.

By contrast, gases at a slightly higher temperature behave more classically, and their mean-field energy is overcome by kinetic energy as the prime source of dynamics in the gas. In such a situation the strength and anisotropy of the dipolar interactions can be made manifest through collisions, rather than through mean-field effects [14]. A very recent experiment showed this explicitly, finding that collisional relaxation of a gas of erbium atoms at ∼400 nK occurred on time scales that varied by a factor of 4, depending on the orientation of the atoms' magnetic dipole moments [15]. This landmark result illustrates the potential for anisotropic dipolar scattering to profoundly influence the kinetics of a cold, thermal gas, from rethermalization and relaxation to viscosity and the propagation of sound, to name but a few features.

In this article we construct a model of the cold, nondegenerate dipolar gas by numerically solving the Boltzmann equation. The model is based on the direct simulation Monte Carlo (DSMC) algorithm [16,17], which is appropriate to the dilute limit found in experiments, when the mean-free path $\lambda_{\rm mf}$ of the atoms in the gas is comparable to or larger than the characteristic scale L of the gas (i.e., Knudsen number $\mathrm{Kn} \equiv \lambda_{\rm mf}/L \gtrsim 1$). Using this model, we explore the thermal relaxation and damping of a dipolar gas that is suddenly taken out of equilibrium. Where applicable, our results are in excellent agreement with the return to equilibrium of the erbium gas in Ref. [15] and, in particular, describe the dependence of the relaxation rate on the polarization direction of the dipoles. Further, we characterize the damping rate of breathing mode oscillations generated in the gas, finding that this damping is also strongly dependent on polarization and is slower than the rethermalization rate. We also evaluate the relevance of mean-field interactions in the gas. Although the density of erbium in the cross-dimensional relaxation experiment was not sufficiently high to observe mean-field effects, we briefly discuss how to modify the DSMC method to include such physics (using particle-in-cell methods for a dipolar Vlasov equation).

The outline of this paper is as follows: In Sec. II we introduce and discuss the details of a cross-dimensional rethermalization experiment which we model. In Sec. III we provide a very brief introduction to the Boltzmann equation and discuss its historical significance in statistical mechanics. Section III B outlines the basic features of our DSMC algorithm, and Sec. III C discusses the differential scattering cross sections for low-energy dipolar interactions. Section IV discusses and quantifies the mean-field interaction in the gas. Section V reports our results for fermions and compares these results to experimental data. Section VI describes similar results, but for bosons. In Sec. VII we draw conclusions and discuss possible avenues for future research.

II. CROSS-DIMENSIONAL RELAXATION OF A DIPOLAR GAS

For concreteness, we here contemplate the experimental situation of Ref. [15]. We employ the notation of that experiment and use the same values of trap frequencies, density, and species (erbium). We stress, however, that the simulations can be made completely general for cold dipolar gas experiments in the thermal regime, including polar molecules.

Experiments involving cross-dimensional relaxation have a long history in cold atoms, going back to the work with cesium [18]. Other experiments include work on Bose-Fermi [19] and Fermi-Fermi [20] mixtures. The experimental scenario we consider is shown in Fig. 1. The gas begins in the equilibrium state of an approximately cylindrically symmetric trap, with the dipole alignment direction in the y-z plane of the laboratory reference frame. The gas is weakly trapped in the y direction and tightly trapped in the x and z directions. The dipole alignment direction, $\hat{\boldsymbol{\epsilon}}$, makes an angle β with the y axis.

Over a (fast) time scale $t_{\rm ramp}$, the trapping frequency along the y axis is significantly increased, sending the system out of equilibrium. The atoms, whose distribution is initially still elongated along the y direction, gain extra momentum along this direction (over the time scale of a quarter trap period). Rethermalization requires the redistribution of this

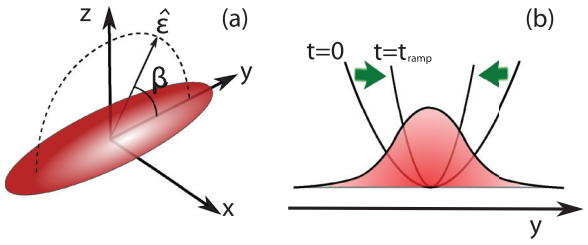

FIG. 1. (Color online) (a) The initial state of the gas, where the atoms occupy the equilibrium state of an approximately cylindrically symmetric trap, elongated in the y direction. The dipole alignment direction is given by $\hat{\boldsymbol{\epsilon}}$. (b) The experiment begins when the trap frequency in the y direction is *suddenly* increased, sending the system out of equilibrium. Rethermalization dynamics depends on the angle β between the dipole alignment direction and the y axis.

additional momentum or potential energy in the y direction into the x and z directions. Due to the highly anisotropic nature of the dipole-dipole interaction, the rate at which this rethermalization (redistribution) occurs depends strongly on the angle, β, between the dipole alignment direction and the y axis (see Fig. 1).

This experiment was recently performed in Innsbruck [15], as a very beautiful demonstration of the standards in precision and control over cold-atomic systems. The atomic species used was ^{167}Er (a fermion), which has the exceptionally large magnetic dipole moment of $7\mu_B$, where μ_B is the Bohr magneton (compared to ^{87}Rb, with $1\mu_B$, and ^{52}Cr, with $6\mu_B$, ^{164}Dy has $10\mu_B$). The experiment began with an initial temperature of 426 nK. Relative to the density of the system, this corresponds to the regime $\bar{n}\lambda_T^3 \approx 0.25$, where $\bar{n}$ is the average density in the trap and $\lambda_T = \hbar\sqrt{2\pi/(mk_BT)}$ is the thermal de Broglie wavelength. In this sense, the system (although cold) is not *deeply* within a regime of quantum degeneracy. This, then, implies that the classical Boltzmann equation should provide the appropriate theoretical description. This being said, quantum-mechanical effects may indeed be a source of error in our simulations, and we attempt to quantify this in Sec. V D.

In spite of this (relatively) low phase-space density, the system is still sufficiently cold that the ratio between the thermal de Broglie wavelength and a characteristic dipole-length scale, $a_d = C_{dd}m/(8\pi\hbar^2)$ (where $C_{dd} = \mu_0\mu^2$ for magnetic dipoles and $C_{dd} = d^2/\epsilon_0$ for electric dipoles, μ_0 and ϵ_0 are, respectively, the permeability and permittivity of the vacuum, and μ and d are the magnetic and electric dipole moments) is $\lambda_T/a_d \approx 39$. From this, we conclude that the two-body scattering physics is strongly within the quantum regime, and the differential scattering cross sections are chosen accordingly [14].

III. THE BOLTZMANN EQUATION FOR DIPOLAR GASES AND THE DSMC METHOD

A. General considerations

The ability to trap and cool atoms with large magnetic dipole moments, such as chromium [21,22], dysprosium [23,24], and erbium [25], provide exciting possibilities for observing novel many-body states (for a recent example, see Ref. [26]). Dipolar molecules are another source of potentially even stronger interactions in dipolar gases [13,27–31]. Developing theoretical tools to understand dipolar gases is currently a very active area of research [8,32–37].

A particularly challenging task in many-body physics is to develop theoretical methods for treating out-of-equilibrium physics. To this end, we report on our progress towards a general tool for simulating out-of-equilibrium dynamics of the normal dipolar gas. Our approach is based on the Boltzmann equation, which we solve using the DSMC algorithm. The motivation for using DSMC typically occurs when the assumptions of fluid mechanics (which generally centers around some form of the Navier-Stokes equation) break down, and one must account for the granular nature of matter (usually, although not exclusively, via statistical mechanics). Bird's DSMC algorithm has evolved over recent decades into a remarkably versatile and useful tool which has been applied across seemingly disparate fields of research [38,39].

Stochastic particle methods, such as the DSMC, have been applied to ultracold gases in a number of previous works. For instance, a variation of the method we describe here was used to study evaporative cooling en route to Bose condensation [40]. In Ref. [41], collisions between two thermal clouds near a d-wave resonance were simulated. The results compared very nicely to experiment [42]. Other examples include the study of collective modes in finite-temperature dynamics [43–45], sympathetic cooling of molecules [46], and degenerate Fermi gas dynamics [47]. To our knowledge, our work is the first time that dipolar differential cross sections have been used [14]. This reduces the efficiency of the DSMC by introducing a rejection-sampling algorithm to sample the differential cross sections. However, we find that numerical convergence is still easily attainable with standard commodity hardware.

The classical Boltzmann equation describes the statistical mechanics of particles in a many-body system with two-body elastic collisions. Its modern derivation typically involves truncation of the BBGKY hierarchy [48] such that two-body (and higher) distribution functions factorize into products of single-body distribution functions (this assumption was referred to by Boltzmann as the *stosszahlansatz*, or the assumption of molecular chaos). The equation for a single-component gas reads

$$\left[\frac{\partial}{\partial t} + \frac{\mathbf{p}}{m}\cdot\nabla_{\mathbf{r}} + \mathbf{F}\cdot\nabla_{\mathbf{p}}\right] f = C[f], \tag{1}$$

where $f = f(\mathbf{r},\mathbf{p};t)$ is the single-particle phase-space distribution, i.e., $f d^3\mathbf{r}d^3\mathbf{p}$ is the expected number of atoms within the phase-space volume $(\mathbf{r},\mathbf{p}) \to (\mathbf{r}+d^3\mathbf{r},\mathbf{p}+d^3\mathbf{p})$, m is the particle mass, $\mathbf{F}$ denotes the external forces acting on the system, i.e., $\mathbf{F} = -\nabla_{\mathbf{r}}U(\mathbf{r},t)$, where $U(\mathbf{r},t)$ is some external potential (trapping potential), and finally,

$$C[f] = \int\frac{d^3\mathbf{p}_1}{m}\int d\Omega\frac{d\sigma}{d\Omega}|\mathbf{p}-\mathbf{p}_1|[f'f_1' - ff_1] \tag{2}$$

is the collision integral. We have used the common notation $f_1^{(\prime)} = f(\mathbf{r},\mathbf{p}_1^{(\prime)};t)$. In principle, one may wish to include a mean-field contribution in the external potential. We discuss the relative importance of this mean-field term in Sec. IV and

demonstrate its insignificance for the purpose of simulating the experiment in Ref. [15].

The collision integral in Eq. (1) provides a mechanism for rethermalization via two-body collisions. Two particles (coinciding at point $\mathbf{r}$) collide with momenta $\mathbf{p}$ and $\mathbf{p}_1$ and emerge from the collision with momenta $\mathbf{p}'$ and $\mathbf{p}'_1$. Net energy and momentum are conserved in the collision, meaning that

$$\mathbf{P} = \mathbf{P}', \tag{3a}$$

$$|\mathbf{p}_{\rm rel}| = |\mathbf{p}'_{\rm rel}|, \tag{3b}$$

where $\mathbf{P}^{(\prime)} = (\mathbf{p}^{(\prime)} + \mathbf{p}_1^{(\prime)})/2$ and $\mathbf{p}_{\rm rel}^{(\prime)} = \mathbf{p}^{(\prime)} - \mathbf{p}_1^{(\prime)}$ denote the center-of-mass and the relative momentum, respectively. The differential cross section

$$\frac{d\sigma}{d\Omega} = \frac{d\sigma}{d\Omega}(\mathbf{p}_{\rm rel}, \mathbf{p}'_{\rm rel}) \tag{4}$$

contains information regarding the likelihood of two particles colliding (given an incident relative momentum $\mathbf{p}_{\rm rel}$) and the likelihood of a postcollision relative momentum given by $\mathbf{p}'_{\rm rel}$. Intriguingly, cross sections which exhibit time-reversal symmetry, that is, $\frac{d\sigma}{d\Omega}(\mathbf{p}_{\rm rel}, \mathbf{p}'_{\rm rel}) = \frac{d\sigma}{d\Omega}(\mathbf{p}'_{\rm rel}, \mathbf{p}_{\rm rel})$, yield irreversible dynamics in the Boltzmann equation as demonstrated by Boltzmann's famous H theorem [49]. The relevant differential cross section for dipolar particles has been derived and discussed in detail in a recent article [14], and we briefly summarize the necessary results in Sec. III C.

Analytic solutions to the Boltzmann equation are difficult to come by [49,50]. An important exception are the well-known equilibrium solutions, the Maxwell-Boltzmann distribution,

$$f(\mathbf{r},\mathbf{p};t) = f_{\rm MB}(\mathbf{r},\mathbf{p}) := \frac{N}{Z}\exp\left[-\frac{p^2/2m + U(\mathbf{r})}{k_B T}\right], \tag{5}$$

where k_B is Boltzmann's constant, T is the temperature, N is the total number of particles, and $Z = \int d^3\mathbf{r} d^3\mathbf{p} \exp[-\frac{p^2/2m+U(\mathbf{r})}{k_B T}]$ gives the correct normalization. Using the conservation laws in Eq. (3), it is straightforward to see that $C[f_{\rm MB}] = 0$, and $f_{\rm MB}$ is a stationary solution to Eq. (1).

We wish to solve the Boltzmann equation, (1), under the following dynamical scenario: Starting from an equilibrium initial distribution, Eq. (5), we change the trapping potential $U(\mathbf{r},t) = \frac{1}{2}m[\omega_x^2 x^2 + \omega_y(t)^2 y^2 + \omega_z^2 z^2]$, where

$$\omega_y(t) = \begin{cases} \omega_y^{(0)}, & t < 0, \\ \sqrt{1 + s\frac{t}{t_{\rm ramp}}}\,\omega_y^{(0)}, & 0 < t \leqslant t_{\rm ramp}, \\ \sqrt{1+s}\,\omega_y^{(0)}, & t > t_{\rm ramp}, \end{cases} \tag{6}$$

such that, over the ramp time $t_{\rm ramp}$, the trap frequency in the y direction is changed by a factor $\sqrt{1+s}$. The choice of square-root dependence on time corresponds to linearly increasing the laser power in an optical dipole trap. The spatial anisotropy, created by the dipole-alignment direction, creates a bias for scattering into particular momentum states. This has implications for the rate of rethermalization, which becomes dependent on the angle between the y axis and the dipole alignment direction. We investigate the rethermalization dynamics as a function of this angle and compare it to the experimental work in Ref. [15].

Attempting to solve the Boltzmann equation by discretizing the temporal axis and the phase-space dimensions is a futile exercise, as (for all but the most trivial cases) one will always run out of computational resources before numerical convergence is achieved. Viable alternatives to find an approximate solution in a close-to-equilibrium scenario do exist, however. For instance, the so-called *method of moments* approach was used in Ref. [36] to study collective excitations of two-dimensional (2D) dipolar fermions in a perturbative limit. In Ref. [51] a variational method was employed to predict relaxation behavior in s-wave interacting gases. Our method is more generally applicable to a wider variety of far-from-equilibrium scenarios, although it is more numerically intense than other methods.

B. The DSMC method

The starting point for the DSMC approximates the distribution function f, by $N_{\rm T}$ test particles, each with position and momenta $[\mathbf{r}_i, \mathbf{p}_i]$ which are found by randomly sampling $f(\mathbf{r},\mathbf{p};t=0)$. That is,

$$f(\mathbf{r},\mathbf{p};0) \approx \xi \sum_{i=1}^{N_{\rm T}} \delta(\mathbf{r} - \mathbf{r}_i)\delta(\mathbf{p} - \mathbf{p}_i), \tag{7}$$

where $\xi = N/N_{\rm T}$ is the ratio of real particles to test particles. The goal is to force the test particles to evolve in time $[\mathbf{r}_i(t), \mathbf{p}_i(t)]$ such that their relationship to f, shown in Eq. (7), remains true at all times. The computational complexity thus increases with $N_{\rm T}$.

On time scales, Δt, much shorter than the mean collision time, the evolution of each test particle is given by its classical trajectory in the potential. Assuming that Δt is also much shorter than the trap period, this is well approximated using a predictor-corrector (symplectic integrator) method,

$$\mathbf{q}_i = \mathbf{r}_i(t) + \frac{\Delta t}{2m}\mathbf{p}_i(t), \tag{8a}$$

$$\mathbf{p}_i(t+\Delta t) = \mathbf{p}_i(t) + \mathbf{F}_i \Delta t, \tag{8b}$$

$$\mathbf{r}_i(t+\Delta t) = \mathbf{q}_i + \frac{\Delta t}{2m}\mathbf{p}_i(t+\Delta t), \tag{8c}$$

where $\mathbf{F}_i = -\nabla_{\mathbf{q}_i} U(\mathbf{q}_i, t)$ is the external force acting on the ith test particle. This is often referred to as the free-streaming dynamics. Note that, if the classical trajectory of a single particle in the trap can be solved analytically (which is obviously straightforward in the case of a harmonic potential), then Eqs. (8) can be replaced with this analytic solution. This provides an advantage in that Δt need not be small compared to the trap period (but still must remain small compared to the mean collision time). In effect, Eqs. (8) account for the left-hand side of the Boltzmann equation as shown in Eq. (1).

In order to include the effects of the collision integral [on the right-hand side of Eq. (1)], a spatial grid is introduced, and the test particles are binned into the volume elements ΔV of this grid. This grid needs to be chosen carefully. The size of the volume element effectively represents the finite resolution of the δ function in our numerics. For this reason it needs to be small since all physical quantities will be coarse-grained over this volume element. However, we use the population of test particles within each volume element to stochastically check

for collisions, and therefore, the volume element must be large enough to contain multiple test particles (in order to obtain reliable statistics). Being certain that one has the necessary combination of *large enough* N_{T} and *small enough* ΔV is an important numerical convergence test.

Once the spatial grid has been established, we check $N_\nu(N_\nu-1)/2$ pairs of particles within the νth volume element (N_ν is the population of the νth volume element). In this step, the computational complexity acquires a N_ν^2 dependence, and simulations will become unfeasible if individual volume elements contain too many test particles. The collision probability is given by

$$P_{ij} = \xi \frac{\Delta t}{m \Delta V} |\mathbf{p}_{\mathrm{rel}}| \sigma(\mathbf{p}_{\mathrm{rel}}), \tag{9}$$

where $\mathbf{p}_{\mathrm{rel}} = \mathbf{p}_i(t) - \mathbf{p}_j(t)$ and

$$\sigma(\mathbf{p}_{\mathrm{rel}}) = \int d\Omega_{\mathbf{p}'_{\mathrm{rel}}} \frac{d\sigma}{d\Omega}(\mathbf{p}_{\mathrm{rel}}, \mathbf{p}'_{\mathrm{rel}}) \tag{10}$$

is the total cross section (as a function of the relative momentum between particle i and particle j), found by integrating the differential cross section over all solid angles of the scattered relative momentum. Computational parameters must be chosen such that $P_{ij} \ll 1$. The collision proceeds if $R < P_{ij}$, where R is a randomly generated number, with a uniform distribution between 0 and 1. If the collision proceeds, we establish the postcollision relative momentum $\mathbf{p}'_{\mathrm{rel}}$ by treating the differential cross section $\frac{d\sigma}{d\Omega}$ as a probability distribution for $\mathbf{p}'_{\mathrm{rel}}$ and stochastically sample it using a rejection-sampling algorithm (see the Appendix for more details). The center-of-mass momentum is conserved during the collision. In this way, at each time step in our simulation, collisions are stochastically implemented, in correct accordance with the total cross section, the local density, the local velocity distribution, and the differential scattering.

Our numerical algorithm described here has some subtle inferiorities compared to certain other algorithms described in the literature. Deficiencies include the absence of locally adaptive spatial grids (to efficiently account for dramatic variations in spatial density), scaled collision probabilities (without which the number of operations in the algorithm scales as $\sim N_{\mathrm{T}}^2$, rather than a potential $\sim N_{\mathrm{T}}$ scaling), and locally adaptive time steps [41,52]. However, the cold-atomic vapors under current consideration have relatively small numbers of particles, and we have thoroughly tested for, and found, excellent numerical convergence in all of our simulations. For this reason, we do not implement the complete set of modern sophistications within the DSMC.

C. Differential scattering in dipolar gases

The cross-section formulas used in this work were derived in Ref. [14] using the Born approximation for the scattering amplitude between two dipolar particles, with dipole moments aligned along the alignment direction $\hat{\boldsymbol{\epsilon}}$ (we use the hat to denote a unit vector). The formulas are $\frac{d\sigma_{\mathrm{F,B}}}{d\Omega}(\mathbf{p}_{\mathrm{rel}}, \mathbf{p}'_{\mathrm{rel}}) = a_d^2 |g_{\mathrm{F,B}}(\mathbf{p}_{\mathrm{rel}}, \mathbf{p}'_{\mathrm{rel}})|^2$, where

$$g_{\mathrm{F}}(\mathbf{p}_{\mathrm{rel}}, \mathbf{p}'_{\mathrm{rel}}) = \frac{1}{\sqrt{2}} \frac{4(\hat{\mathbf{p}}_{\mathrm{rel}}.\hat{\boldsymbol{\epsilon}})(\hat{\mathbf{p}}'_{\mathrm{rel}}.\hat{\boldsymbol{\epsilon}}) - 2[(\hat{\mathbf{p}}_{\mathrm{rel}}.\hat{\boldsymbol{\epsilon}})^2 + (\hat{\mathbf{p}}'_{\mathrm{rel}}.\hat{\boldsymbol{\epsilon}})^2](\hat{\mathbf{p}}_{\mathrm{rel}}.\hat{\mathbf{p}}'_{\mathrm{rel}})}{1 - (\hat{\mathbf{p}}_{\mathrm{rel}}.\hat{\mathbf{p}}'_{\mathrm{rel}})^2}, \tag{11a}$$

$$g_{\mathrm{B}}(\mathbf{p}_{\mathrm{rel}}, \mathbf{p}'_{\mathrm{rel}}) = \frac{1}{\sqrt{2}} \left[-2\frac{a}{a_d} - \frac{2(\hat{\mathbf{p}}_{\mathrm{rel}}.\hat{\boldsymbol{\epsilon}})^2 + 2(\hat{\mathbf{p}}'_{\mathrm{rel}}.\hat{\boldsymbol{\epsilon}})^2 - 4(\hat{\mathbf{p}}_{\mathrm{rel}}.\hat{\boldsymbol{\epsilon}})(\hat{\mathbf{p}}'_{\mathrm{rel}}.\hat{\boldsymbol{\epsilon}})(\hat{\mathbf{p}}_{\mathrm{rel}}.\hat{\mathbf{p}}'_{\mathrm{rel}})}{1 - (\hat{\mathbf{p}}_{\mathrm{rel}}.\hat{\mathbf{p}}'_{\mathrm{rel}})^2} + \frac{4}{3} \right], \tag{11b}$$

a_d is the dipole length scale given by $a_d = m\mu_0\mu^2/(8\pi\hbar^2)$, μ_0 is the vacuum permeability, μ is the atomic magnetic dipole moment ($\mu = 7\mu_B$ in the case of erbium), and a is the s-wave scattering length. The subscripts F and B, respectively, correspond to fermionic and bosonic symmetry constraints (^{167}Er, which was used in the experiment [15], is fermionic).

The total cross section, which we use to evaluate the collision probability in Eq. (9), can also be evaluated analytically [14],

$$\sigma_{\mathrm{F}}(\mathbf{p}_{\mathrm{rel}}) = a_d^2 \frac{\pi}{3}[3 + 18\cos^2(\eta) - 13\cos^4(\eta)] \tag{12a}$$

$$\sigma_{\mathrm{B}}(\mathbf{p}_{\mathrm{rel}}) = a_d^2 \frac{\pi}{9}\{72a^2 - 24a[1 - 3\cos^2(\eta)] + 11 - 30\cos^2(\eta) + 27\cos^4(\eta)\}, \tag{12b}$$

where $\eta = \cos^{-1}(\hat{\mathbf{p}}_{\mathrm{rel}}.\hat{\boldsymbol{\epsilon}})$ is the angle between the dipole alignment direction and the incoming relative momentum. Equation (12) [12(a) or 12(b), depending on whether the collision pair is identical fermions or bosons] is used in Eq. (9) to evaluate the likelihood of a collision.

Once it has been established that the collision does or does not occur, the postcollision relative velocity is found by sampling the distribution function,

$$P_{\mathrm{F,B}}(\theta_{\mathrm{rel}}, \phi_{\mathrm{rel}}; \eta) = \frac{1}{\sigma_{\mathrm{F,B}}(\mathbf{p}_{\mathrm{rel}})} \frac{d\sigma_{\mathrm{F,B}}}{d\Omega}(\mathbf{p}_{\mathrm{rel}}, \mathbf{p}'_{\mathrm{rel}}) \sin\theta_{\mathrm{rel}}. \tag{13}$$

Note that we only need to sample θ_{rel} and ϕ_{rel} since η is given to us by the (already known) incoming relative momentum of the collision pair. The *collision reference frame* $(x_{\mathrm{cf}}, y_{\mathrm{cf}}, z_{\mathrm{cf}})$ is defined such that the z_{cf} axis points along the direction of $\mathbf{p}_{\mathrm{rel}}$, and the dipole-alignment direction $\hat{\boldsymbol{\epsilon}}$ lies in the x_{cf}-z_{cf} plane. The purpose of defining and operating within the collision reference frame is to make the analytic formulas Eqs. (11a) and (11b) as wieldy as possible. The coordinates θ and ϕ in Eq. (13) are the polar and azimuthal angles, respectively, of $\mathbf{p}'_{\mathrm{rel}}$ in the collision reference frame. We (arbitrarily) decide to include the factor $\sin\theta$ in the definition of the probability distribution function (rather than the metric) such that $\int_0^{2\pi} d\phi \int_0^{\pi} d\theta\, P_{\mathrm{F,B}}(\theta, \phi; \eta) = 1$. Sampling the probability distribution in Eq. (13) is not simple, so we use a rejection sampling algorithm which we describe in the Appendix.

To convert between the laboratory reference frame and the collision reference frame, we find

$$\begin{aligned}\mathbf{e}_1^{\rm cf} &= [\cos(\gamma)\cos(\phi_{\rm rel})\cos(\theta_{\rm rel}) - \sin(\gamma)\sin(\phi_{\rm rel})]\,\mathbf{e}_1^{\rm lf} \\ &+ [\cos(\gamma)\sin(\phi_{\rm rel})\cos(\theta_{\rm rel}) - \sin(\gamma)\cos(\phi_{\rm rel})]\,\mathbf{e}_2^{\rm lf} \\ &- \cos(\gamma)\sin(\theta_{\rm rel})\mathbf{e}_3^{\rm lf}, \end{aligned} \tag{14}$$

$$\begin{aligned}\mathbf{e}_2^{\rm cf} &= [-\sin(\gamma)\cos(\phi_{\rm rel})\cos(\theta_{\rm rel}) - \cos(\gamma)\sin(\phi_{\rm rel})]\,\mathbf{e}_1^{\rm lf} \\ &+ [\cos(\gamma)\cos(\phi_{\rm rel}) - \sin(\gamma)\sin(\phi_{\rm rel})\cos(\theta_{\rm rel})]\,\mathbf{e}_2^{\rm lf} \\ &+ \sin(\gamma)\sin(\theta_{\rm rel})\mathbf{e}_3^{\rm lf}, \end{aligned} \tag{15}$$

$$\mathbf{e}_3^{\rm cf} = \cos(\phi_{\rm rel})\sin(\theta_{\rm rel})\mathbf{e}_1^{\rm lf} + \sin(\phi_{\rm rel})\sin(\theta_{\rm rel})\mathbf{e}_2^{\rm lf} + \cos(\theta_{\rm rel})\mathbf{e}_3^{\rm lf}, \tag{16}$$

where the angle

$$\begin{aligned}\gamma = \operatorname{acot}\{&\cos(\theta_{\rm rel})\cot(\phi_\varepsilon - \phi_{\rm rel}) \\ &- \cot(\theta_\varepsilon)\csc(\phi_\varepsilon - \phi_{\rm rel})\sin(\theta_{\rm rel})\} \end{aligned} \tag{17}$$

and

$$\hat{\mathbf{p}}_{\rm rel} = \sin(\theta_{\rm rel})\cos(\phi_{\rm rel})\mathbf{e}_1^{\rm lf} + \sin(\theta_{\rm rel})\sin(\phi_{\rm rel})\mathbf{e}_2^{\rm lf}\cos(\theta_{\rm rel})\mathbf{e}_3^{\rm lf}, \tag{18}$$

$$\hat{\boldsymbol{\varepsilon}} = \sin(\theta_\varepsilon)\cos(\phi_\varepsilon)\mathbf{e}_1^{\rm lf} + \sin(\theta_\varepsilon)\sin(\phi_\varepsilon)\mathbf{e}_2^{\rm lf} + \cos(\theta_\varepsilon)\mathbf{e}_3^{\rm lf}. \tag{19}$$

We have used the common notation where $\mathbf{e}_{1,2,3}^{\rm lf,cf}$ denote the standard (unit) basis vectors of Euclidean space in either the laboratory (lf) or the collision (cf) frame. The symbols θ_ε and ϕ_ε refer to the azimuthal and polar angles, respectively, of the dipole alignment direction in the laboratory frame, as shown in Eq. (19).

IV. DISCUSSION OF THE MEAN-FIELD INTERACTION

In a more general situation the inclusion of a mean-field interaction may be desirable [53,54]. This requires an alteration of the Boltzmann equation, (1), such that $\mathbf{F} = -\boldsymbol{\nabla} U(\mathbf{r},t)$ now consists of two parts, $U(\mathbf{r},t) = U_{\rm ext}(\mathbf{r},t) + U_{\rm mf}(\mathbf{r},t)$, an external potential $U_{\rm ext}$ and a mean-field potential $U_{\rm mf}$. Such an approach may be dubbed a dipolar Vlasov equation, in recognition of its similarity to the Vlasov equation used in plasma physics [55]. The mean-field potential is a dynamical variable (away from equilibrium) found from the convolution

$$U_{\rm mf}(\mathbf{r},t) = \int d^3\mathbf{r}' n(\mathbf{r}',t) V_{\rm dd}(\mathbf{r}-\mathbf{r}'), \tag{20}$$

where $n(\mathbf{r},t) = \int d^3\mathbf{p}\; f(\mathbf{r},\mathbf{p};t)$ is the spatial number density and $V_{\rm dd}(\mathbf{r})$ is the dipolar interaction between two particles separated by $\mathbf{r}$. This is given by

$$V_{\rm dd}(\mathbf{r}) = \frac{C_{\rm dd}}{4\pi}\frac{1-3(\hat{\mathbf{r}}\cdot\hat{\boldsymbol{\varepsilon}})^2}{r^3}. \tag{21}$$

In general it is certainly true that the physics associated with the mean-field interaction can have a strong influence.

Upon including the mean-field potential, the effects of interactions manifest within two distinct terms of the Boltzmann equation. The natural question arises whether or not there is some error akin to double-counting due to the presence of both these terms. The collision term describes an instantaneous collision between exactly two particles within the gas, such that momentum is exchanged between these two particles. This effect is entirely local and occurs irrespective of the other particles in the gas. On the other hand, the mean field consists of a collective effect due to every single particle in the gas. In this sense the two terms are conceptually distinct. Serious problems begin to occur when the mean-field interaction energy becomes particularly significant (taking up a large fraction of the total energy in the gas). In this situation, the collisions can begin to occur, on the background not of a translationally invariant potential energy landscape (as is generally assumed [14]) but, rather, of an appreciably varying potential energy landscape, caused by the mean field of nearby particles. These problems arise when typical values of na_d^3 approach or exceed unity. As we show below, this is not the case in our current realm of interest.

In order to ascertain the relevance of the mean field in Eq. (20) for our current simulation, we wish to consider the total mean-field energy per particle $e_{\rm mf}$ in the gas and compare this to the temperature. That is, we calculate

$$e_{\rm mf} = \frac{1}{2N}\int d^3{\rm r}\; n(\mathbf{r},t)U_{\rm mf}(\mathbf{r},t). \tag{22}$$

We are only interested in placing an approximate upper bound on the value of $e_{\rm mf}$, so we simplify the situation at hand by assuming that the density of the gas (at any given time) is given by a Gaussian distribution with cylindrical symmetry about the dipole-alignment direction, which (solely for the purpose of this discussion) we assume to be along the z axis:

$$n(\mathbf{r}) = \frac{N}{(2\pi)^{3/2}\sigma_\perp^2\sigma_z}\exp\left[-\frac{x^2+y^2}{2\sigma_\perp^2} - \frac{z^2}{2\sigma_z^2}\right]. \tag{23}$$

One could perform a more realistic calculation in the absence of cylindrical symmetry, but analytic calculations are difficult in this case. Although a numerical solution is not difficult, it changes the result only by a factor of order unity and is, therefore, not of interest to us at this stage. The wonderfully elegant Fourier transform of $V_{\rm dd}(\mathbf{r})$ allows for the analytic calculation of $e_{\rm mf}$ [10],

$$e_{\rm mf} = -\frac{N}{48\sqrt{\pi^3}}\frac{C_{\rm dd}}{\sigma_\perp^2\sigma_z}h\left(\frac{\sigma_\perp}{\sigma_z}\right), \tag{24}$$

where

$$h(x) = \frac{1+2x^2}{1-x^2} - \frac{3x^2\operatorname{arctanh}\sqrt{1-x^2}}{(1-x^2)^{3/2}} \tag{25}$$

is a function generally of order unity [although $h(1) = 0$ since the angular average of $V_{\rm dd}$ is 0]. In an attempt to draw some broad conclusions, we simply consider the prefactor in $e_{\rm mf}$ and compare it to the temperature:

$$\kappa = \frac{1}{k_B T}\frac{N}{48\sqrt{\pi^3}}\frac{C_{\rm dd}}{\sigma_\perp^2\sigma_z}. \tag{26}$$

In the experiment in Ref. [15] which we are currently interested in, the quantity κ is never more than $\kappa \lesssim 0.02$, indicating that physics associated with the mean field is likely to be insignificant, at least to the first level of approximation.

In other situations (involving higher densities or larger dipole length scales), where κ becomes appreciably large,

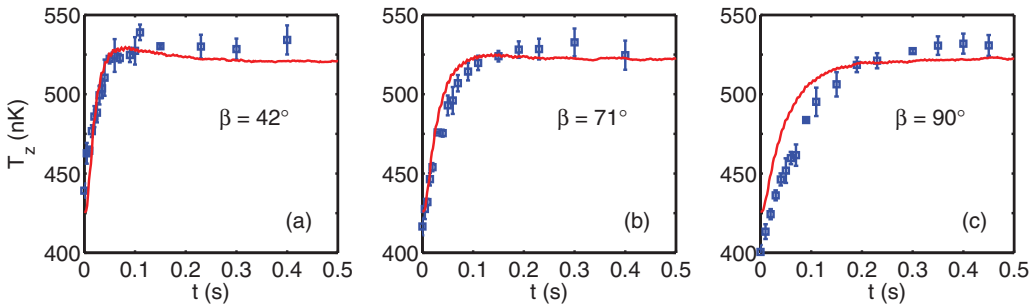

FIG. 2. (Color online) A comparison between the experimentally measured rethermalization process and the results from the DSMC simulation. (a–c) The solid (red) line shows the result of the DSMC simulation, calculated analagously to Eq. (28), but along the z axis. Experimental data points are shown by (blue) squares with error bars. The agreement is reasonable, especially considering that there was no postprocessing of the experimental data or any adjustments to the theory in order to produce these fits (no free parameters).

incorporating the mean field into the simulation may be necessary. The computational issues of doing so are, to a certain extent, manageable (see, for example, the vast literature on *particle-in-cell* methods used to solve the ordinary Vlasov equation in the field of plasma physics [56]). Briefly, the process involves binning the particles in position space to find the density $n(\mathbf{r},t)$, smoothing the density via convolution with a suitably chosen Gaussian kernel, and then calculating the potential, using Eq. (20), and, ultimately, the force $\mathbf{F}$ [56]. For issues relating to clarity, we currently wish to relegate further details of this procedure to a future publication.

V. RESULTS FOR FERMIONS

The physical parameters chosen in our simulation are taken directly from Ref. [15]. These are as follows.

$N = 8 \times 10^4$	Total atom number
$T = 426$ nK	Initial temperature
$m = 2.77 \times 10^{-25}$ kg	^{167}Er mass
$a_d = 5.25$ nm	^{167}Er dipole length scale
$\omega_x = 2\pi \times 393$ Hz $\omega_y^{(0)} = 2\pi \times 38$ Hz $\omega_z = 2\pi \times 418$ Hz	Initial trap
$t_{\text{ramp}} = 14$ ms	Ramp time
$s = 1.8$	Final trap, y axis [see Eq. (6)]

We vary the computational parameters N_{T} and ΔV until numerical convergence is achieved. This typically occurred when $N_{\text{T}} \approx N$, although we perform our simulations right through to $N_{\text{T}} = 4 \times N$ to thoroughly check the convergence. We find that these simulations converge rather rapidly with ΔV [57], however, we perform simulations right through to $\bar{n}\Delta V = 0.35$ (where $\bar{n}$ is the initial trap-averaged density), with $N_{\text{T}} = 4 \times N$, to be certain of convergence.

A. Anisotropic pseudotemperature

To evaluate the rate of rethermalization, we find the standard deviations of the test-particle distributions; for instance,

$$\sigma_x(t) = \sqrt{\frac{1}{N_{\text{T}}}\sum_{i=1}^{N_{\text{T}}} x_i(t)^2}, \quad \sigma_{p_x}(t) = \sqrt{\frac{1}{N_{\text{T}}}\sum_{i=1}^{N_{\text{T}}} p_{xi}(t)^2},$$

and equally for the y and z directions. We note that a Gaussian distribution provides a reasonably accurate approximation to the instantaneous empirical distribution of test particles in the simulation. However, the moments above are well defined, regardless of whether or not this is the case. From these standard deviations, we can define a time-dependent, anisotropic *pseudotemperature*, related to the widths of the test-particle distribution function in each direction, relative to the instantaneous value of the trapping parameters; for instance,

$$\mathcal{T}_x = \frac{m\omega_x^2\sigma_x^2}{k_B}, \quad \mathcal{T}_{p_x} = \frac{\sigma_{p_x}^2}{mk_B}, \tag{27}$$

and equally for the y and z axes. This definition makes particular sense in the case of a Gaussian distribution. The two quantities $\mathcal{T}_x$ and $\mathcal{T}_{p_x}$, above, can be combined into a single pseudotemperature in the x direction (or in any direction) given by the mean,

$$T_x = \frac{\mathcal{T}_x + \mathcal{T}_{p_x}}{2}. \tag{28}$$

The results of this analysis for the temperature along the z axis are shown in Fig. 2, along with the experimental data from Ref. [15]. A more complete set of results, for the temperatures in all three directions, is shown in Fig. 3. An interesting observation we make is the apparent nonmonotonic rethermalization behavior of T_z near $\beta = 45°$ (this behavior seems to exist right through $30° \lesssim \beta \lesssim 60°$). This behavior was not observed in the experiment, likely due to the fact that it is a subtle effect which may be difficult to measure. Indeed we note in Fig. 2(a) that the scatter and error bars for the experimental data points appear to be of a similar size to, or even larger than, the magnitude of the nonmonotonic *hump* in the theoretical result.

B. Analyzing the rate of rethermalization as a function of β

In order to define the rate of rethermalization it is customary to fit an exponential decay curve to the equilibration dynamics shown in Figs. 2 and 3. For example, in the z direction, one would write $T_z(t) = T_z^{(\text{eq})} + \Delta T_z e^{-t/\tau_z}$, where $T_z^{(\text{eq})}$ (a fit parameter) is the equilibrated temperature, and $T_z^{(\text{eq})} + \Delta T_z$ is the initial temperature (426 nK in our case). The time constant of this exponential decay curve, τ_z, is then written as

$$\tau_z = \frac{\alpha_z}{\bar{n}\bar{\sigma}_{\text{F,B}}\bar{v}}, \tag{29}$$

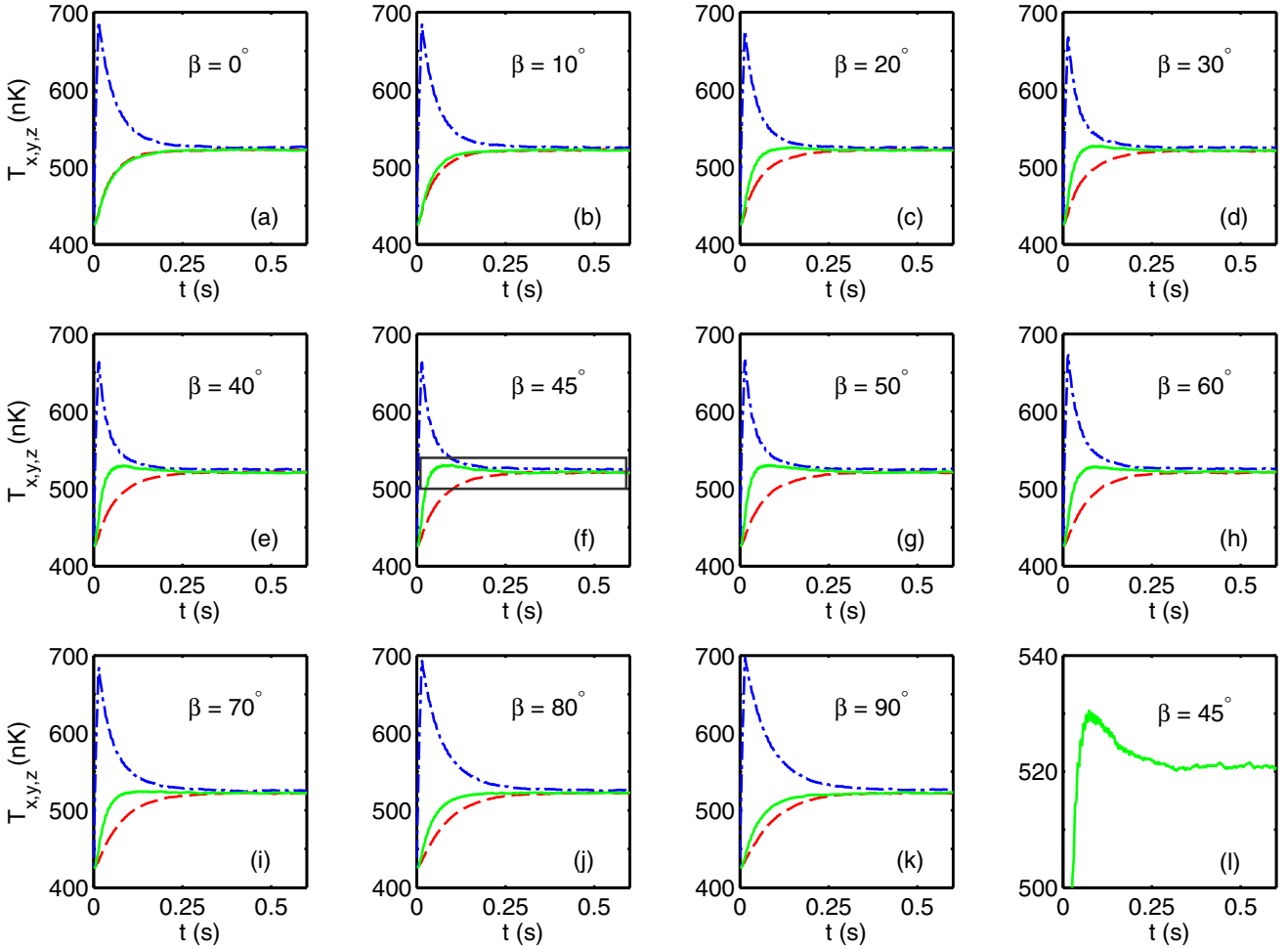

FIG. 3. (Color online) Pseudotemperatures along the x axis [dashed (red) line], y axis [dot-dashed (blue) line], and z axis [solid (green) line] defined analogously to Eq. (28). In the first 14 ms (the ramp time), the temperature along the y axis increases as a result of the rapid change in the trap frequency along this direction. After 14 ms, the system relaxes down towards the new equilibrium state. The rate at which T_x, T_y, and T_z return to an equilibrium value displays a strong dependence on β, which we explore further in Sec. V B. An unexpected feature we observe is the nonmonotonic path by which T_z returns to equilibrium near $\beta = 45°$. The effect is shown in greater detail in (l) by zooming in on the relevant part of (f). This is certainly an interesting consequence of the anisotropic dipole differential scattering, but note that the behavior only occurs along one of the coordinate axes (the z axis in this case), and overall there is *no* violation of Boltzmann's H theorem.

where $\bar{v} = \sqrt{16k_BT/\pi m}$ is the mean velocity in the gas, and $\bar{\sigma}_{\mathrm{F,B}}$ is the total cross section of Eq. (12) averaged over all solid angles of the incoming relative momentum $\mathbf{p}_{\mathrm{rel}}$, such that $\bar{\sigma}_{\mathrm{F}} = (32\pi/15)a_d^2$ and $\bar{\sigma}_{\mathrm{B}} = 8\pi a^2 + (32\pi/45)a_d^2$. In this way, the quantity $\bar{n}\bar{\sigma}_{\mathrm{F,B}}\bar{v}$ represents the mean collision frequency in the gas, and the quantity α can be conceptually thought of as the *number of collisions required for rethermalization*. The exact same procedure can be applied to the x and y axes. In our current situation $\alpha_{x,y,z}$ will be a function of the angle β between the dipole-alignment direction and the y axis. The results, which agree well with experimental data from Ref. [15], are shown in Fig. 4.

It should be noted that Refs. [14,15] compute α_z in a simpler way, by approximating the short-time behavior of the dynamics via the Enskog equation [58]. This has also shown adequate agreement with the data but gives considerably less detail than the present DSMC simulations.

C. Trap oscillations and covariances in position and momentum space

The sudden change in the trap frequency along the y axis gives rise to a breathing mode along this direction (see Ref. [59]

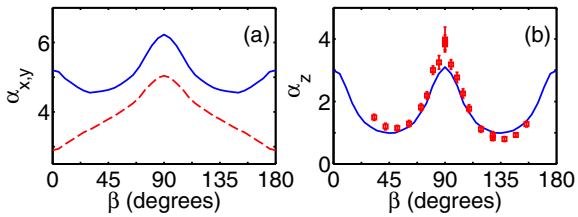

FIG. 4. (Color online) α (number of collisions required for rethermalization) as a function of the angle β along (a) the x direction [dashed (red) line] and y direction [solid (blue) line] and (b) the z direction. Data in (b) were taken from the experiment in Ref. [15] (data not taken in the x and y directions).

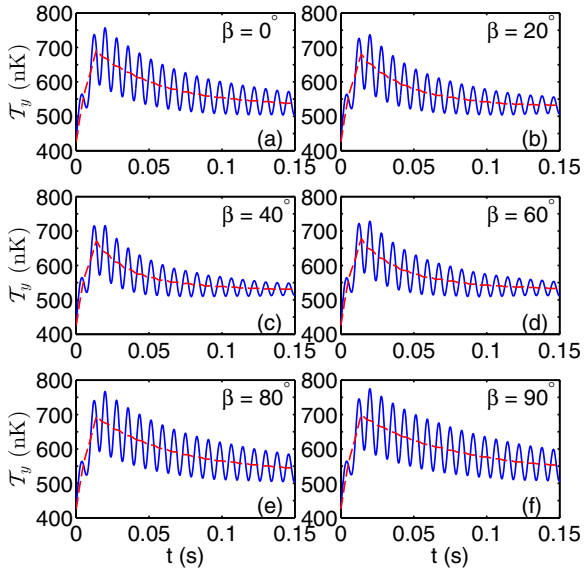

FIG. 5. (Color online) The rapid change in trapping frequency along the y axis generates a large breathing mode along this direction. This is here in plots of $\mathcal{T}_y$ versus time for a variety of values of β. These breathing modes exist also in the momentum distribution, $\mathcal{T}_{p_y}$, and look identical to these plots except that the oscillations are exactly π radians out of phase (leading to the monotonic behavior in T_y shown in Fig. 3). The dashed (red) line in each of the figures represents T_y. We use Eq. (30) as a fit to the decay of this breathing mode. The breathing mode dynamics along the x and z axes are barely noticeable in our simulations.

for a discussion of this subject in the case of a classical gas with hard-sphere interactions). The oscillations are apparent in either the position variable $\mathcal{T}_y$ or the momentum variable $\mathcal{T}_{p_y}$, but *not* in the sum T_y, which is plotted in Fig. 3 (since $\mathcal{T}_{p_y}$ and $\mathcal{T}_y$ oscillate exactly out of phase with each other). This behavior is shown in Fig. 5. The experiment in Ref. [15] neither reported nor searched for any evidence of these oscillations or their damping periods (data were only analyzed along the z axis). The frequency of the breathing mode is $2\omega_y (t > t_{\rm ramp})$ [39,50]. Collisions will eventually cause this mode to damp out (intriguingly, though, monopole modes are undamped in spherically symmetric harmonic traps). In order to quantify this, we subtract the pseudotemperature [shown by the dashed (red) line in Fig. 5] and fit a decaying sinusoid to the data:

$$\mathcal{T}_y(t) - T_y(t) \approx A e^{-t/\tau_{\rm osc}} \sin[\omega t + \delta]\,. \tag{30}$$

In the current experimental scenario the erbium gas lies firmly within the collisionless limit (the trap frequency is significantly higher than the mean collision frequency), and therefore the oscillation frequency is $\omega = 2\sqrt{1+s}\,\omega_y^{(0)}$, i.e., twice the final trap frequency. Of course, if, instead, the experiment were in the hydrodynamic regime, rather than the collisionless regime, this would not be the case [59,60]. We only fit to the region $t > t_{\rm ramp}$ when the trap is no longer changing. The parameters A, $\tau_{\rm osc}$, and δ are all fitting parameters. We then scale the time constant $\tau_{\rm osc}$ by the collision frequency to give us

$$\tau_{\rm osc} = \frac{\alpha_{\rm osc}}{\bar{n}\bar{\sigma}_{\rm F,B}\bar{v}}, \tag{31}$$

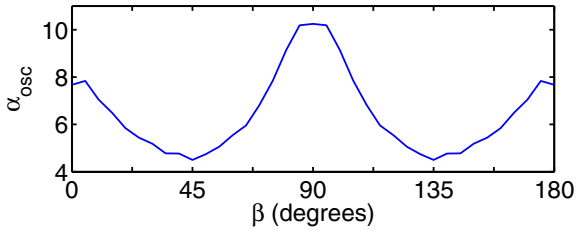

FIG. 6. (Color online) The breathing mode along the y axis is damped over a time scale $\tau_{\rm osc}$ found from Eqs. (30) and (31). The dependence on β is shown. Note the qualitative similarity of $\alpha_{\rm osc}$ (shown above) to α_y in the solid (blue) line in Fig. 4(a). However, the oscillations take considerably longer to damp than the envelope, as $\alpha_{\rm osc} > \alpha_y$.

such that we can loosely interpret $\alpha_{\rm osc}$ as the *number of collisions required for the breathing mode to damp out*. Naively one might expect this to be the same as the α in Sec. V B, and indeed we find distinct similarities, however, the breathing mode takes considerably longer to damp out (a factor of 2 or more). The results for how $\alpha_{\rm osc}$ depends on β are shown in Fig. 6; note the qualitative similarity between Fig. 6 and the solid (blue) line in Fig. 4(a). We do not find that the other fitting parameters, A and δ, have any significant dependence on β. However, A does depend on the size of the perturbation to the trap, and δ depends on the ramp time $t_{\rm ramp}$ (this is apparent in the instantaneous quench, for which analytic formulas are straightforward).

In contrast, breathing modes along the x and z axis are considerably less pronounced [61]. This is simply due to the fact that the perturbing force on the system in this situation is entirely along the y axis (see Fig. 1).

If the quench were performed instantaneously, a simple analytic solution is available in the extreme-collisionless limit,

$$f(\mathbf{r},\mathbf{p},t) = f_{\rm MB}^{(2{\rm D})}[(x,z),(p_x,p_z)] \times \mathcal{M}\exp\left[-\frac{1}{2}(y \quad p_y)\mathbf{\Phi}(t)^{-1}\begin{pmatrix} y \\ p_y\end{pmatrix}\right], \tag{32}$$

where $f_{\rm MB}^{(2{\rm D})}$ is the 2D Maxwell-Boltzmann distribution (along the x and z axes), $\mathcal{M}$ is a normalization constant, and the covariance matrix

$$\mathbf{\Phi} = \begin{pmatrix} \zeta & \eta \\ \eta & \theta \end{pmatrix} \tag{33}$$

is such that $\zeta = \langle y^2\rangle - \langle y\rangle^2$, $\eta = \langle y p_y\rangle - \langle y\rangle\langle p_y\rangle$, and $\theta = \langle p_y^2\rangle - \langle p_y\rangle^2$. Note that ζ and θ are proportional to the pseudotemperatures $\mathcal{T}_y$ and $\mathcal{T}_{p_y}$, respectively, whereas η is the covariance between position and momentum space. Ignoring collisions in the system, these variances evolve according to [61]

$$\zeta = \frac{\zeta_0}{2}\left[1 + \Gamma + (1-\Gamma)\cos\left(2\omega_y^{(\rm f)}t\right)\right], \tag{34a}$$

$$\eta = \frac{\sqrt{\zeta_0\theta_0}}{2}[\Gamma^{1/2} - \Gamma^{-1/2}]\sin\left(2\omega_y^{(\rm f)}t\right), \tag{34b}$$

$$\theta = \frac{\theta_0}{2}\left[1 + \Gamma^{-1} + (1-\Gamma^{-1})\cos\left(2\omega_y^{(\rm f)}t\right)\right], \tag{34c}$$

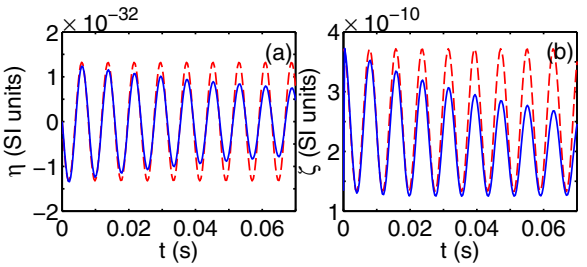

FIG. 7. (Color online) Comparison between the DSMC simulation for an instantaneous quench and the analytic formulas in Eqs. (34). (a) Covariance between position and momentum space; (b) variance in position space (proportional to $\mathcal{T}_y$). These particular data are for the dipole alignment direction of $\beta = 0$. The DSMC simulation is shown by the solid (blue) line; the analytic formulas, by the dashed (red) line. The analytic formulas do an excellent job of correctly predicting the amplitude and phase of the oscillations. For this ratio of collision-to-trap frequency, the damping becomes appreciable, of the order of several trap periods.

where $\zeta_0 = k_B T/[m(\omega_y^{(0)})^2]$ and $\theta_0 = k_B T m$ are the initial spatial and momentum variances, respectively, and $\Gamma = (\omega_y^{(0)}/\omega_y^{(f)})^2$ is the ratio of initial-to-final trap frequencies (squared).

We have performed simulations of the cross-dimensional relaxation procedure in the case of an instantaneous quench. The results are shown in Fig. 7, where we compare the simulation data to the analytic formulas, Eqs. (34). The simulations reveal the increasing importance of collision-induced damping for times beyond several trap periods. The decay rate of the covariance η depends on the dipole angle β. To within the numerical accuracy of these simulations, we find that the rate at which η decays, and the dependence this decay has on β, is extremely close to that for ζ and θ (the pseudotemperatures) shown in Fig. 6.

D. Quantum many-body effects

The Boltzmann equation, as written in Eq. (1), treats the many-body dynamics of the system entirely in terms of classical mechanics. For our comparison with the experiment in Ref. [15], this may conceivably be a source of error. In 1928, Nordheim made adjustments to the Boltzmann equation to account for the quantum-mechanical effects of Fermi blocking and Bose enhancement [62]. The net result of Nordheim's work was an alteration to the collision integral,

$$C_N[f] = \int \frac{d^3\mathbf{p}_1}{m} \int d\Omega \frac{d\sigma}{d\Omega} |\mathbf{p} - \mathbf{p}_1| [f' f_1' (1 \pm h^3 f)(1 \pm h^3 f_1) - f f_1 (1 \pm h^3 f')(1 \pm h^3 f_1')], \quad (35)$$

where h is Planck's constant, and the plus sign applies to identical bosons (Bose enhancement) while the minus sign applies to identical fermions (Fermi blocking). From this point of view, the quantum many-body effects in the system are determined by the phase-space density (see Ref. [63] for a discussion of, and recent results on, a fermionic gas), specifically how many particles occupy a volume of phase space equal to h^3. If this number is much less than 1, quantum effects should be small; if this number is comparable to 1, quantum effects will

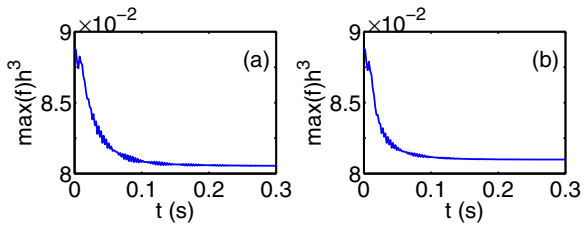

FIG. 8. (Color online) The (maximum) number of particles in a volume element of phase space equal to h^3 as a function of time for two separate dipole-alignment angles: (a) $\beta = 0$ and (b) $\beta = 45$. The phase-space density decreases as the system equilibrates to a higher final temperature. From this, we estimate that quantum many-body effects are indeed small enough to be neglected (at least as a first approximation).

be important. The maximum phase-space density is plotted in Fig. 8 as a function of time for two values of β. From this, we conclude that quantum many-body effects will have a negligible effect on the dynamics at this temperature. This goes some way in explaining the reasonably good agreement between our theory and the experiment in this case. We do not expect our theory to provide quantitative accuracy at significantly lower temperatures, although modifying our algorithm to account for the mechanism of Bose enhancement or Fermi blocking is a future goal of this project. Speculating further on this, we note that the Boltzmann-Nordheim equation will have not only a (potentially) different path to equilibrium, but also (at lower temperatures) a different equilibrium state (the famous Bose-Einstein and Fermi-Dirac distributions). How this would affect the dependence of $\alpha_{x,y,z}$ on β is an interesting and open question.

VI. RESULTS FOR BOSONS

It is very straightforward to repeat these simulations for a system of bosons simply by replacing g_F with g_B in

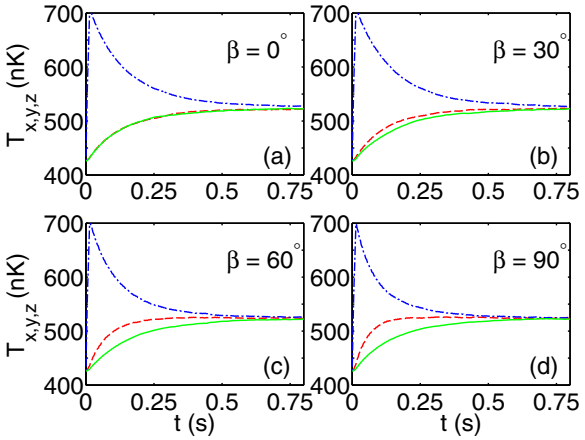

FIG. 9. (Color online) Pseudotemperatures along the x axis [dashed (red) line], y axis [dot-dashed (blue) line], and z axis [solid (green) line] as a function of time for the bosonic dipole scattering cross section. Experimental data were not taken for this case, but we observe that the rethermalization rates show a strong dependence on β (particularly along the x axis).

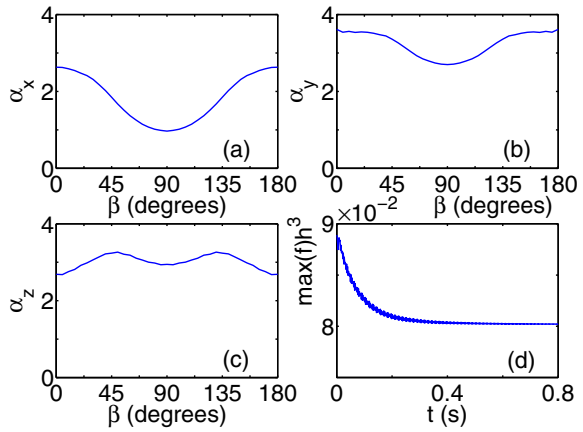

FIG. 10. (Color online) (a) α_x, (b) α_y, and (c) α_z (number of collisions required for rethermalization) as a function of β in the case of bosons. (d) Maximum phase-space density as a function of time for $\beta = 30^\circ$.

the differential scattering cross section and $\sigma_F \to \sigma_B$ [see Eqs. (11a), (11b), and (12)]. We choose to keep the geometry of the trap, the atomic species, and the number of particles the same as that was used in Sec. V for fermions. We set the s-wave scattering length $a = 0$, to emphasize the peculiarities of the anisotropic dipolar differential scattering. The distinctions between bosonic and fermionic scattering behavior naturally alters details of the rejection sampling algorithm (see Appendix) and changes the results, but there is no conceptual change in what we are doing, so we provide less detail than we did for fermions. In addition, experimental data do not yet exist for bosons, so we cannot make the same comparisons in that respect.

Figure 9 shows the rethermalization of the pseudotemperatures for bosons (analagous to Fig. 3 for fermions). Somewhat ironically, in the context of low-energy scattering, the rethermalization procedure takes approximately three times longer for bosons than for fermions with the same density and dipole moment. This is due to the factor-of-3 difference (for $a = 0$) between the angularly averaged total cross sections $\bar{\sigma}_F$ and $\bar{\sigma}_B$ [14]. Increasing the s-wave scattering length a would naturally change this situation. The nature of the differential cross sections is such that a nonmonotonic rethermalization process is not observed for bosons [as it is in Fig. 3(l)]. Figures 10(a)–10(c) shows the *number of collisions required for rethermalization* as a function of β. In Fig. 10(d) we show the maximum phase-space density as a function of time for the case $\beta = 30^\circ$. Again, this indicates that the Boltzmann equation should provide an approximately accurate theoretical description at these densities and temperatures. Figure 11 shows the *number of collisions required to damp out the breathing mode*. Note the qualitative similarity between α_{osc} in Fig. 11 and α_y in Fig. 10(b), but with a quantitative difference of approximately a factor of 2.

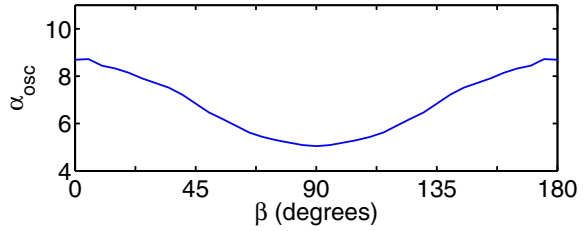

FIG. 11. (Color online) Decay of the breathing mode along the y axis in the case of bosons. Again, there is a strong qualitative similarity between this curve and the curve in Fig. 10(b), but an important quantitative difference is that α_{osc} is larger by a factor of ≈ 2.

VII. CONCLUSIONS AND DISCUSSION

In this article we have developed a DSMC numerical algorithm to solve the Boltzmann equation for an ultracold dipolar gas. We have used this method to study the cross-dimensional relaxation dynamics of a dipolar gas via a full simulation of the phase-space dynamics. Where applicable, we have compared our numerical results with the experimental data in Ref. [15] and found favourable agreement. This suggests that the DSMC algorithm provides a quantitative method for understanding the normal component in a dipolar gas. This is a promising result. The method is suitable for both fermions and bosons, although experimental data currently exist only for fermions. The method and results direct our interest toward a new regime where interactions in the gas manifest from collisions rather than the mean field.

More specifically, we have studied the damping of trap breathing modes in the system and quantified the pronounced dependence of rethermalization on the dipole-alignment direction. We find that the breathing mode takes significantly longer (approximately a factor of 2) to decay than the envelope for rethermalization, which is found by averaging over momentum-space and real-space dynamics.

Our current work is entirely focused on the thermal gas, above quantum degeneracy. There are several reasons why understanding this normal component of an ultracold dipolar gas is important. For instance, attractive interactions along the dipole alignment direction (due to the mean field) can destabilize the system [2,4,64,65]. Thermal energy can counteract this instability [5,66], therefore we expect the normal component to have a qualitative, as well as a quantitative, role in the dynamics. Our method presented here, if combined or coupled with one of the many low-temperature theories (e.g., [67,68]), would constitute a complete finite-temperature description of dipolar gases (in the same vein as the Zaremba-Nikuni-Griffin formalism of regular Bose condensates [43,69,70]). This remains as work in progress.

The method used in this paper (DSMC) is a remarkably versatile tool, potentially capable of simulating a multitude of out-of-equilibrium scenarios. Extending it into a regime where many-body quantum mechanical behavior becomes prevalent (beyond the simple two-body scattering level, which plays such a vital role in our current work) is the direction in which we intend to take this research. Possible avenues for doing so include incorporating the effects of Bose stimulation and Pauli blocking into the differential scattering cross sections, as prescribed by Nordheim (see Eq. (35) in Ref. [62]). This requires modifications to the DSMC algorithm, which were originally introduced in the context of nuclear equations of state, particularly during heavy-ion collisions [48,71]. The

basic ideas have seen application in ultracold-atomic systems of fermions (see Refs. [72,73]). Another possibility, perhaps more relevant for bosonic systems, involves coupling the Boltzmann equation (the purely classical version may suffice) to an equation describing the superfluid component in the system. For example, one could consider using the well-known Gross-Pitaevskii equation [70] or the more sophisticated *c*-field techniques [67].

ACKNOWLEDGMENTS

A.G.S. wishes to thank Andrew Wade and Blair Blakie for useful advice in developing the DSMC code. A.G.S. and J.L.B. both wish to thank Francesca Ferlaino and Kiyotaka Aikawa for sending us their experimental data and providing useful feedback on our work. A.G.S. and J.L.B. also acknowledge interesting discussions with Benjamin Lev, Yijun Tang, Nathaniel Burdick, and Kristian Baumann regarding dysprosium gases. We acknowledge funding from the Air Force Office of Scientific Research under the Multidisciplinary University Research Initiative Grant No. FA9550-1-0588, and the JILA Physics Frontier Center.

APPENDIX: REJECTION SAMPLING ALGORITHM

The procedure of rejection sampling is not new [74], but for completeness, we provide a brief description of the details specific to our situation. A more thorough description of the algorithm in general can be found in Ref. [75].

1. Fermions

To sample from $P_{\mathrm{F}}(\theta,\phi;\eta)$ defined in Eq. (13), the strategy is to start from a simpler distribution (which is easy to sample)—call it $g(\theta,\phi) = 1/(2\pi^2)$—and (appropriately) reject those samples which were *unlikely* [recall that we only need to sample θ and ϕ since η is given to us by the (already known) incoming relative momentum of the collision pair]. The algorithm goes as follows:

(i) Sample $(\bar{\theta},\bar{\phi})$ from $g(\theta,\phi)$, and sample u from $\mathcal{U}(0,1)$ (the uniform distribution over the unit interval).

(ii) Check whether $u < P_{\mathrm{F}}(\bar{\theta},\bar{\phi};\eta)/[Mg(\bar{\theta},\bar{\phi})]$, where M is an *upper bound* such that $M > P_{\mathrm{F}}(\theta,\phi;\eta)/g(\theta,\phi)$ for all θ and ϕ.

(iii) If step ii holds true, accept $(\bar{\theta},\bar{\phi})$ as a realization of P_{F}. If it does not hold true, reject $(\bar{\theta},\bar{\phi})$, and start over at step i.

In order to find the upper bound $M(\eta)$ we transform to the collision reference frame, where

$$P_{\mathrm{F}}(\theta,\phi;\eta) = \frac{6\sin(\theta)[\cos(\theta)(\cos^2(\eta)-\cos^2(\phi)\sin^2(\eta))+\cos(\phi)\sin(\theta)\sin(2\eta)]^2}{\pi(3+18\cos^2(\eta)-13\cos^4(\eta))}. \tag{A1}$$

Using standard optimization methods, we find that the maximum value of $P_{\mathrm{F}}(\theta,\phi;\eta)$ occurs at $\phi_{\max}=0$, and

$$\theta_{\max} = \begin{cases} \operatorname{acos}\left(\frac{\sqrt{7+\cos(4\eta)-\sqrt{2\sin^2(\eta)(17-\cos(4\eta))}}}{2\sqrt{3}}\right), & \eta<\pi/4 \quad \text{or} \quad \pi/2<\eta<3\pi/4; \\ \operatorname{acos}\left(-\frac{\sqrt{7+\cos(4\eta)-\sqrt{2\sin^2(\eta)(17-\cos(4\eta))}}}{2\sqrt{3}}\right), & \pi/4<\eta<\pi/2 \quad \text{or} \quad 3\pi/4<\eta. \end{cases} \tag{A2}$$

From this, we define $M = 2\pi^2 P_{\mathrm{F}}^{(\max)}(\eta)$, where

$$P_{\mathrm{F}}^{(\max)}(\eta) = \frac{6\cos^2(\theta_{\max}-2\eta)\sin(\theta_{\max})}{\pi(3+18\cos^2\eta-13\cos^4\eta)}. \tag{A3}$$

2. Bosons

The procedure for bosons is essentially equivalent, except with

$$P_{\mathrm{B}}(\theta,\phi;\eta) = \frac{2\sin(\theta)[-2+3\cos^2(\eta)+3\cos^2(\phi_{\max})\sin^2(\eta)]^2}{\pi(11-30\cos^2(\eta)+27\cos^4(\eta))}, \tag{A4}$$

$\theta_{\max}=\pi/2$,

$$\phi_{\max} = \begin{cases} 0, & \eta<\operatorname{atan}(\sqrt{2}) \quad \text{or} \quad \eta>\pi-\operatorname{atan}(\sqrt{2}), \\ \pi/2, & \operatorname{atan}(\sqrt{2})<\eta<\pi-\operatorname{atan}(\sqrt{2}), \end{cases} \tag{A5}$$

and

$$P_{\mathrm{B}}^{(\max)}(\eta) = \frac{2[-2+3\cos^2\eta+3\cos^2\phi_{\max}\sin^2\eta]^2}{\pi(11-30\cos^2\eta+27\cos^4\eta)}. \tag{A6}$$

Note that P_{B} in Eq. (A4) factorizes into a product of two functions involving only θ and only ϕ. This was not the case for the fermionic cross section; see Eq. (A1). This allows for the sampling algorithm to be more efficient in the case of bosons than it is for fermions, since θ can be sampled directly.

[1] T. Lahaye, T. Koch, B. Fröhlich, M. Fattori, J. Metz, A. Griesmaier, S. Giovanazzi, and T. Pfau, Nature **448**, 672 (2007).

[2] T. Koch, T. Lahaye, J. Metz, B. Fröhlich, A. Griesmaier, and T. Pfau, Nat. Phys. **4**, 218 (2008).

[3] S. Müller, J. Billy, E. A. L. Henn, H. Kadau, A. Griesmaier, M. Jona-Lasinio, L. Santos, and T. Pfau, Phys. Rev. A **84**, 053601 (2011).

[4] U. R. Fischer, Phys. Rev. A **73**, 031602(R) (2006).

[5] R. N. Bisset, D. Baillie, and P. B. Blakie, Phys. Rev. A **83**, 061602(R) (2011)

[6] L. Santos, G. V. Shlyapnikov, and M. Lewenstein, Phys. Rev. Lett. **90**, 250403 (2003).

[7] R. M. Wilson, S. Ronen, J. L. Bohn, and H. Pu, Phys. Rev. Lett. **100**, 245302 (2008).

[8] J. P. Corson, R. M. Wilson, and J. L. Bohn, Phys. Rev. A **87**, 051605(R) (2013).

[9] R. N. Bisset and P. B. Blakie, Phys. Rev. Lett. **110**, 265302 (2013).

[10] T. Lahaye, C. Menotti, L. Santos, M. L. Lewenstein, and T. Pfau, Rep. Prog. Phys. **72**, 126401 (2009).

[11] C. Ticknor, R. M. Wilson, and J. L. Bohn, Phys. Rev. Lett. **106**, 065301 (2011).

[12] C. Ticknor, Phys. Rev. A **86**, 053602 (2012).

[13] B. Yan, S. A. Moses, B. Gadway, J. P. Covey, K. R. A. Hazzard, A. M. Rey, D. S. Jin, and J. Ye, Nature **501**, 521 (2013).

[14] J. L. Bohn and D. S. Jin, Phys. Rev. A **89**, 022702 (2014).

[15] K. Aikawa, A. Frisch, M. Mark, S. Baier, R. Grimm, J. L. Bohn, D. S. Jin, G. M. Bruun, and F. Ferlaino, Phys. Rev. Lett. **113**, 263201 (2014).

[16] G. A. Bird, *Molecular Gas Dynamics* (Clarenden Press, Oxford, UK, 1994).

[17] G. A. Bird, *The DSMC Method*, Version 1.2 (University of Sydney, Sydney, 2013).

[18] C. R. Monroe, E. A. Cornell, C. A. Sackett, C. J. Myatt, and C. E. Wieman, Phys. Rev. Lett. **70**, 414 (1993).

[19] J. Goldwin, S. Inouye, M. L. Olsen, and D. S. Jin, Phys. Rev. A **71**, 043408 (2005).

[20] L. Costa, J. Brachmann, A.-C. Voigt, C. Hahn, M. Taglieber, T. W. Hänsch, and K. Dieckmann, Phys. Rev. Lett. **105**, 123201 (2010).

[21] A. Griesmaier, J. Werner, S. Hensler, J. Stuhler, and T. Pfau, Phys. Rev. Lett. **94**, 160401 (2005).

[22] Q. Beaufils, R. Chicireanu, T. Zanon, B. Laburthe-Tolra, E. Maréchal, L. Vernac, J.-C. Keller, and O. Gorceix, Phys. Rev. A **77**, 061601 (2008).

[23] M. Lu, S. H. Youn, and B. L. Lev, Phys. Rev. Lett. **104**, 063001 (2010).

[24] M. Lu, N. Q. Burdick, S. H. Youn, and B. L. Lev, Phys. Rev. Lett. **107**, 190401 (2011).

[25] K. Aikawa, A. Frisch, M. Mark, S. Baier, A. Rietzler, R. Grimm, and F. Ferlaino, Phys. Rev. Lett. **108**, 210401 (2012).

[26] X. Cui, B. Lian, T.-L. Ho, B. L. Lev, and H. Zhai, Phys. Rev. A **88**, 011601(R) (2013).

[27] K.-K. Ni, S. Ospelkaus, M. H. G. de Miranda, A. Pe'er, B. Neyenhuis, J. J. Zirbel, S. Kotochigova, P. S. Julienne, D. S. Jin, and J. Ye, Science **322**, 231 (2008).

[28] K. Aikawa, D. Akamatsu, J. Kobayashi, M. Ueda, T. Kishimoto, and S. Inouye, New J. Phys. **11**, 055035 (2009).

[29] K.-K. Ni, S. Ospelkaus, D. Wang, G. Quemener, B. Neyenhuis, M. H. G. de Miranda, J. L. Bohn, J. Ye, and D. S. Jin, Nature **464**, 1324 (2010).

[30] T. Takekoshi, L. Reichsöllner, A. Schindewolf, J. M. Hutson, C. R. Le Sueur, O. Dulieu, F. Ferlaino, R. Grimm, and H.-C. Nägerl, Phys. Rev. Lett. **113**, 205301 (2014).

[31] B. Pasquiou, A. Bayerle, S. M. Tzanova, S. Stellmer, J. Szczepkowski, M. Parigger, R. Grimm, and F. Schreck, Phys. Rev. A **88**, 023601 (2013).

[32] C. Ticknor, Phys. Rev. A **88**, 013623 (2013).

[33] C. Ticknor, Phys. Rev. A **89**, 053601 (2014).

[34] D. Baillie and P. B. Blakie, arXiv:1407.4252.

[35] K. Pawłowski, P. Bienias, T. Pfau, and K. Rzazewski, Phys. Rev. A **87**, 043620 (2013).

[36] M. Babadi and E. Demler, Phys. Rev. A **86**, 063638 (2012).

[37] S. S. Natu and R. M. Wilson, Phys. Rev. A **88**, 063638 (2013).

[38] To name but a very select few of the many applications of DSMC we point out its application in microelectromechanical systems [A. Frangi, C. Cercignani, S. Mukherjee, and N. Aluru (eds.), *Advances in Multiphysics Simulation and Experimental Testing of MEMS*, 1st ed. (Imperial College Press, London, 2008)]; volcanic plumes on Io [J. Zhang, D. B. Goldstein, P. L. Varghese, L. Trafton, C. Moore, and K. Miki, Icarus **172**, 479 (2004)]; and helium plasma [D. Breden, K. Miki, and L. L. Raja, Appl. Phys. Lett. **99**, 111501 (2011)].

[39] C. Cercignani, *The Boltzmann Equation and Its Applications* (Springer-Verlag, New York, 1988).

[40] H. Wu, E. Arimondo, and C. J. Foot, Phys. Rev. A **56**, 560 (1997).

[41] A. C. J. Wade, D. Baillie, and P. B. Blakie, Phys. Rev. A **84**, 023612 (2011).

[42] N. R. Thomas, N. Kjaergaard, P. S. Julienne, and A. C. Wilson, Phys. Rev. Lett. **93**, 173201 (2004).

[43] B. Jackson and E. Zaremba, Phys. Rev. A **66**, 033606 (2002).

[44] B. Jackson and E. Zaremba, Phys. Rev. Lett. **87**, 100404 (2001).

[45] B. Jackson and E. Zaremba, Phys. Rev. Lett. **88**, 180402 (2002).

[46] P. Barletta, J. Tennyson, and P. F. Barker, New J. Phys. **12**, 113002 (2010).

[47] F. Toschi, P. Vignolo, S. Succi, and M. P. Tosi, Phys. Rev. A **67**, 041605(R) (2003).

[48] A. Bonasera, F. Gulminelli, and J. Molitoris, Phys. Rep. **243**, 1 (1994).

[49] G. Gallavotti, W. L. Reiter, and J. Yngvason (eds.), *Boltzmann's Legacy* (European Mathematical Society, Zürich, 2008).

[50] D. Guéry-Odelin, J. G. Muga, M. J. Ruiz-Montero, and E. Trizac, Phys. Rev. Lett. **112**, 180602 (2014).

[51] G. M. Kavoulakis, C. J. Pethick, and H. Smith, Phys. Rev. Lett. **81**, 4036 (1998).

[52] A. C. J. Wade, M.S. thesis, University of Otago, 2012.

[53] D. Guéry-Odelin, Phys. Rev. A **66**, 033613 (2002).

[54] P. Pedri, D. Guéry-Odelin, and S. Stringari, Phys. Rev. A **68**, 043608 (2003).

[55] A. A. Vlasov, Sov. Phys. Usp. **10**, 721 (1968).

[56] C. K. Birdsall and A. B. Langdon, *Plasma Physics via Computer Simulation* (McGraw-Hill, New York, 1985).

[57] Convergence in this context refers to the notion of *stochastic convergence*. That is, the result of a single simulation with a given seed of the random number generator shows an *increasing preference* toward a particular pattern. Convergence

has occurred once the discrepancy between this pattern and the single-simulation result is entirely stochastic, since it can then be reduced simply by averaging over different seeds of the random number generator. There exists a vast literature on this subject, see, for instance, P. Billingsley, *Convergence of Probability Measures* (John Wiley and Sons, New York, 1999).

[58] F. Reif, *Fundamentals of Statistical and Thermal Physics* (McGraw–Hill, New York, 1965).

[59] D. Guéry-Odelin, F. Zambelli, J. Dalibard, and S. Stringari, Phys. Rev. A **60**, 4851 (1999).

[60] B. Jackson and E. Zaremba, Phys. Rev. Lett. **89**, 150402 (2002).

[61] L. You and M. Holland, Phys. Rev. A **53**, R1(R) (1996).

[62] L. W. Nordheim, Proc. R. Soc. Lond. A **119**, 689 (1928).

[63] O. Goulko, F. Chevy, and C. Lobo, New J. Phys. **14**, 073036 (2012).

[64] L. Santos, G. V. Shlyapnikov, P. Zoller, and M. Lewenstein, Phys. Rev. Lett. **85**, 1791 (2000).

[65] J. P. Corson, R. M. Wilson, and J. L. Bohn, Phys. Rev. A **88**, 013614 (2013).

[66] C. Ticknor, Phys. Rev. A **85**, 033629 (2012).

[67] P. B. Blakie, A. S. Bradley, M. J. Davis, R. J. Ballagh, and C. W. Gardiner, Adv. Phys. **57**, 363 (2008).

[68] T. P. Billam, P. Mason, and S. A. Gardiner, Phys. Rev. A **87**, 033628 (2013).

[69] E. Zaremba, T. Nikuni, and A. Griffin, J. Low Temp. Phys. **116**, 277 (1999).

[70] A. Griffin, T. Nikuni, and E. Zaremba, *Bose-Condensed Gases at Finite Temperatures* (Cambridge University Press, Cambridge, 2009).

[71] J. Aichelin, Phys. Rep. **202**, 233 (1991).

[72] T. Lepers, D. Davesne, S. Chiacchiera, and M. Urban, Phys. Rev. A **82**, 023609 (2010).

[73] O. Goulko, F. Chevy, and C. Lobo, Phys. Rev. A **84**, 051605(R) (2011).

[74] J. von Neumann, Natl. Bureau Stand. **12**, 36 (1951).

[75] C. Robert and G. Castella, *Monte Carlo Statistical Methods* (Springer, New York, 2004).